Adsorption Rate of Ethanol on Activated Carbon Fiber

Bidyut Baran Saha,*,† Ibrahim I. El-Sharkawy,† Anutosh Chakraborty,† Shigeru Koyama,† Seong-Ho Yoon,‡ and Kim Choon Ng§

Interdisciplinary Graduate School of Engineering Sciences, Kyushu University, Kasuga-koen 6-1, Kasuga-shi, Fukuoka 816-8580, Japan, Institute for Materials Chemistry and Engineering, Kyushu University, Kasuga-koen 6-1, Kasuga-shi, Fukuoka 816-8580, Japan, and Department of Mechanical Engineering, National University of Singapore, 10 Kent Ridge Crescent, Singapore 119260

We have measured experimentally the adsorption kinetics of ethanol on pitch-based activated carbon fibers (ACFs) of type (A-20) at different adsorption temperatures ranging from 27 to 60 °C, which are suitable for adsorption chiller design. These data are unavailable in the literature. The mass uptake of ethanol adsorbed on ACF is measured by a thermogravimetric analyzer (TGA) under a controlled pressure and temperature environment. The uptake mass and temperature measurements are logged with a time interval of 0.5 s making a continuous change of ethanol mass uptake with time. System pressure is kept constant during the adsorption experiments and the adsorption rate of the ACF (A-20)/ethanol pair is estimated within the concentration range of 0.1 and 0.5 kg of adsorbate/kg of ACF. A comparison between the experimentally measured data and the predicted results of adsorption rate shows a good agreement, demonstrating the adsorption rate is mainly controlled by surface diffusion.

Introduction

The physical adsorption process which occurs mainly within the pores and surface of an adsorbent requires knowledge of the adsorption characteristics over wide ranges of pressures and temperatures. Adsorption on a solid adsorbent is the fundamental process in the fields of separation processes,[1−3] purification of gases,[4−6] solar adsorption cooling,[7−8] low-temperature driven advanced adsorption cooling,[9,10] cryocooler,[11,12] and extensive work on hydrogen storage.[13−15] The understanding of thermodynamic property fields of adsorbent plus adsorbate systems is important, because it enables the adsorption process to be analyzed. It is well-known that the pore characteristics (pore volume, surface area, and pore-size distribution) of the adsorbent play an important role in the adsorption characteristics of an adsorbent−refrigerant pair. Some studies on ACFs have been made[16−20] because ACF has the potential of being an excellent working pair for refrigeration application. The BET (Brunauer−Emmet−Teller) surface area and pore size distributions of ACF (A-20) have been determined using N_2 adsorption,[21] where the surface area and total pore volume are found to be 1.93×10^6 m^2/kg and 10.3×10^{-4} m^3/kg, respectively. Moreover, ACFs provide faster adsorption kinetics compared with that of a granular adsorbent.[22−25] The thin-fiber shape clearly ensures fast intraparticle adsorption kinetics compared with pelletized or granular activated carbon commonly employed in gas-phase and aqueous-phase adsorption. This becomes more important in designing adsorption units where intraparticle diffusion resistance is the most significant factor, resulting in a considerable decrease in the size of adsorption units. The fibrous form is also favored because of ease in handling when it is used in felt or fabric forms and of availability in consolidated shapes by recently developed molding techniques.

* Corresponding author. E-mail: bidyutb@cm.kyushu-u.ac.jp.
† Interdisciplinary Graduate School of Engineering Sciences, Kyushu University.
‡ Institute for Materials Chemistry and Engineering, Kyushu University.
§ Department of Mechanical Engineering, National University of Singapore.

Owing to the high performance of the ACF + ethanol pair, it may lead to a compact adsorption unit. From the above perspectives, the main target of this experimental work is to measure the adsorption rate of ethanol on pitch-type ACF of type (A-20). The adsorption process is carried out at different adsorbent temperatures but constant vapor pressure. Mass uptake of ethanol on ACF (A-20) is traced at 0.5 s intervals until the equilibrium conditions are attained in the ACF (A-20)/ethanol system.

Experimental Section

A thermogravimetric analyzer (TGA) apparatus (Cahn TG 2121) is used to measure the adsorption uptake of ethanol on ACF. Figure 1 shows the schematic layout of the experimental apparatus that comprises a reacting chamber, an evaporator, a constant temperature water bath, and a water circulator. Two porous dampers are used at the inlet and outlet of the adsorbate gas to reduce pressure fluctuation in the sample cell from the continuous operations of the vacuum pump and the regulating valve. One K type thermocouple is inserted into the reacting chamber of the TGA apparatus near the bottom of the sample pan to measure the adsorbent temperature. The system pressure is controlled by using a MKS pressure controller (type 651C), and a MKS Baratron pressure sensor (type 631A) records the chamber pressure. To avoid any condensation, a tape type electric heater is mounted at the outer surface of the connecting tubes, maintaining the tube surfaces at 10 to 15 °C above the saturation temperature of the refrigerant vapor.

Adsorption experiments are carried out at constant evaporator temperature, namely, at 15 °C, and the adsorbent temperature varies over a range from 27 to 60 °C by controlling the TGA built-in heater temperature. To protect from any damage of the microbalance that might occur due to the ethanol reaction, a small amount of helium gas is injected from the top of the dome-shaped cover continuously, while the system is kept connected to the vacuum pump at all times during the experiment. Gas extraction from the reacting chamber is conducted from the top

10.1021/je060071z CCC: $30.25
Published on Web 08/02/2006

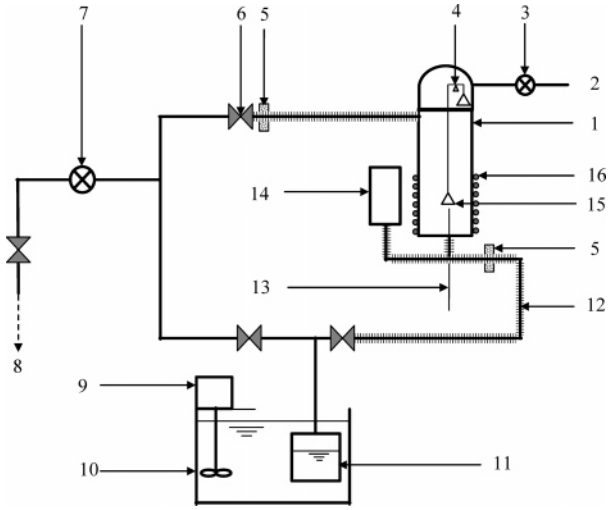

Figure 1. Schematic diagram of the TGA experimental apparatus: 1, reacting chamber; 2, helium injection port; 3, gas flow regulating valve; 4, microbalance; 5, porous mesh (damper); 6, valve; 7, pressure regulating valve; 8, vacuum pump connection; 9, water circulator; 10, water bath; 11, evaporator; 12, tape heater; 13, thermocouple; 14, pressure sensor; 15, sample pan; 16, heater.

Table 1. Composition and Porous Characteristics of ACF (A-20)

elemental analysis				
sample	C (wt %)	H (wt %)	N (wt %)	O (wt %) (difference)
ACF(A-20)	94.48	0.71	0.40	4.41

porous characteristics				
adsorbent	adsorbate	BET surface area (m^2/kg)	total pore volume (m^3/kg)	average pore diameter (Å)
ACF(A-20)	N_2	1.93×10^6	10.28×10^{-4}	21.60

section of the TGA to minimize the mixing of ethanol and helium gases.

The adsorbent sample is regenerated in situ under vacuum conditions at 140 °C to remove all moisture over a period of several hours. The sample is then cooled to the set temperature until the system stability is attained. The valve between the evaporator and the TGA apparatus is opened and the adsorption process starts. After the beginning of the adsorption process, the system pressure increases sharply at a value of 30 mbar. As the evaporator saturation pressure is 43 mbar, the difference in the evaporator pressure and the system pressure occurs due to

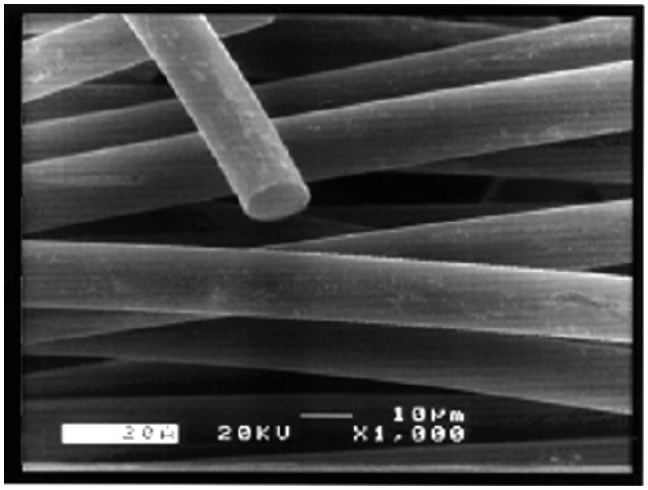

Figure 2. SEM photograph of ACF (A-20).

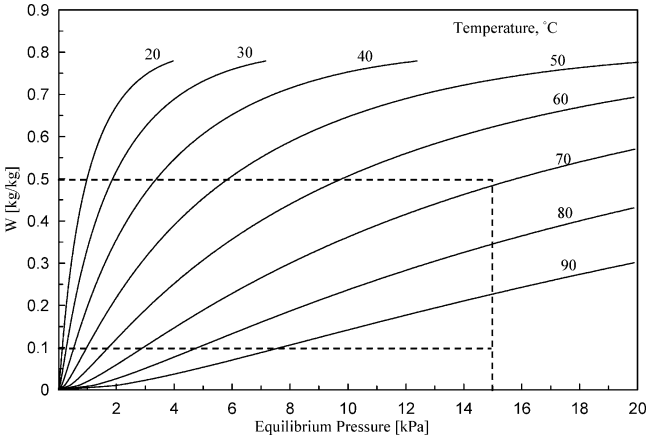

Figure 3. Isotherms of the ACF (A-20)/ethanol pair.

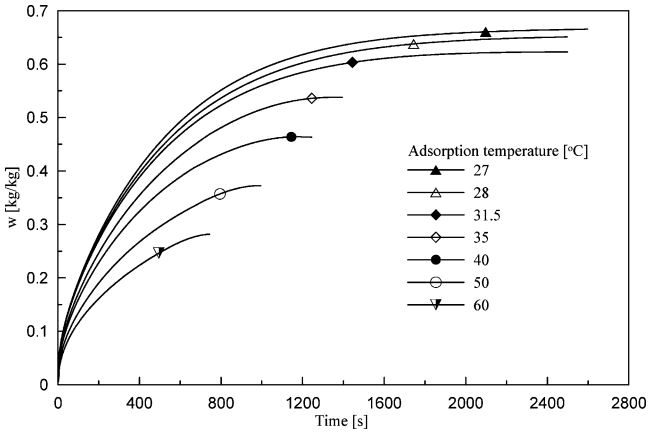

Figure 4. Kinetic uptakes of ethanol on ACF (A-20) at different adsorption temperatures.

the continuous connection of the system with the vacuum pump. The adsorption process is continued until it reaches the equilibrium adsorption condition. The mass of the sample as well as its temperature is recorded with a time interval of 0.5 s. The system pressure is recorded by using a data logger connected to the pressure sensor.

The adsorbent ACF (A-20) is made by spinning in an inert atmosphere using the mesophase carbon melt that was derived from cold tar pitch at high temperatures, and meso- and micropores are prepared by careful activation, a procedure developed by the Unitika Co. Ltd., Japan. Elemental analysis of the ACF (A-20) sample was performed by using inverse gas chromatography. The carbon, hydrogen, and nitrogen contents were determined directly while the oxygen content was calculated by taking the difference (as no ash was found as residue). The porous characteristics (BET surface area, total pore volume, average pore diameter) of the ACF (A-20) sample were evaluated from the adsorption isotherm of N_2 at −196 °C after outgassing at a temperature of 300 °C for 3 h and a residual pressure of 10^{-3} Pa by using the Autosorb 1-MP machine. The detailed elemental analyses and the porous characteristics of the ACF (A-20) sample are furnished in Table 1. As noted in Table 1, the ACF (A-20) has a higher carbon content and possesses a higher surface area as compared with other carbon fibers. The field emission scanning electron micrograph (FE-SEM) of the ACF (A-20) is shown in Figure 2. As can be seen from Figure 2, the fibers have a uniform diameter of around 13 μm.

Uncertainty Analysis. In the TGA apparatus, the mass reading has been measured directly by a microbalance with an accuracy of 0.1 μg. For an initial tare adsorbent sample mass of 71 mg,

Table 2. Experimental Uptake at 27 °C

time/s	w/kg·kg^{-1}	time/s	w/kg·kg^{-1}	time/s	w/kg·kg^{-1}
0	0	1230	0.620967606	2460	0.664526761
30	0.107729577	1260	0.623891549	2490	0.664764789
60	0.148664789	1290	0.626639437	2520	0.664974648
90	0.182108451	1320	0.629230986	2550	0.66518169
120	0.211890141	1350	0.631671831	2580	0.665374648
150	0.238973239	1380	0.633991549	2610	0.665564789
180	0.264214085	1410	0.636159155	2640	0.665759155
210	0.287676056	1440	0.638195775	2670	0.665939437
240	0.309601408	1470	0.640083099	2700	0.666114085
270	0.330228169	1500	0.641846479	2730	0.666266197
300	0.349566197	1530	0.643495775	2760	0.666416901
330	0.367816901	1560	0.645030986	2790	0.666547887
360	0.384980282	1590	0.646477465	2820	0.666694366
390	0.401192958	1620	0.647805634	2850	0.666826761
420	0.416471831	1650	0.649053521	2880	0.666980282
450	0.430947887	1680	0.650233803	2910	0.667088732
480	0.444647887	1710	0.651340845	2940	0.667280282
510	0.457505634	1740	0.652356338	2970	0.667357746
540	0.469911268	1770	0.65331831	3000	0.667460563
570	0.481540845	1800	0.654222535	3030	0.667657746
600	0.492512676	1830	0.655052113	3060	0.667791549
630	0.502764789	1860	0.655822535	3090	0.66788169
660	0.512478873	1890	0.656549296	3120	0.667998592
690	0.521690141	1920	0.657257746	3150	0.668091549
720	0.530391549	1950	0.657930986	3180	0.668174648
750	0.538616901	1980	0.658543662	3210	0.668238028
780	0.546384507	2010	0.659076056	3240	0.668312676
810	0.553669014	2040	0.65958169	3270	0.668371831
840	0.560557746	2070	0.660076056	3300	0.668422535
870	0.567064789	2100	0.660550704	3330	0.668642254
900	0.573177465	2130	0.660997183	3360	0.668735211
930	0.578949296	2160	0.661425352	3390	0.668722535
960	0.584366197	2190	0.661802817	3420	0.668732394
990	0.589514085	2220	0.662188732	3450	0.668753521
1020	0.594340845	2250	0.662573239	3480	0.668780282
1050	0.598874648	2280	0.662907042	3510	0.668808451
1080	0.603128169	2310	0.663208451	3540	0.668842254
1110	0.607153521	2340	0.663487324	3570	0.668856338
1140	0.610929577	2370	0.663766197	3600	0.668876056
1170	0.614469014	2400	0.664050704		
1200	0.617814085	2430	0.66431831		

Table 3. Experimental Uptake at 31.5 °C

time/s	w/kg·kg^{-1}	time/s	w/kg·kg^{-1}
0	0	1230	0.587535211
30	0.105930986	1260	0.590183099
60	0.145550704	1290	0.592743662
90	0.17748169	1320	0.595042254
120	0.206023944	1350	0.597261972
150	0.231894366	1380	0.599298592
180	0.255628169	1410	0.60123662
210	0.277719718	1440	0.603023944
240	0.298305634	1470	0.604666197
270	0.317574648	1500	0.606257746
300	0.335649296	1530	0.607697183
330	0.352622535	1560	0.609080282
360	0.368571831	1590	0.610338028
390	0.383657746	1620	0.611497183
420	0.397905634	1650	0.612566197
450	0.41131831	1680	0.613595775
480	0.424046479	1710	0.614485915
510	0.436038028	1740	0.615367606
540	0.447387324	1770	0.616147887
570	0.458116901	1800	0.616877465
600	0.468252113	1830	00.617547887
630	0.477809859	1860	0.618121127
660	0.486959155	1890	0.618678873
690	0.495694366	1920	0.619192958
720	0.503749296	1950	0.619676056
750	0.511340845	1980	0.62003662
780	0.518509859	2010	0.6204
810	0.525305634	2040	0.6207
840	0.531716901	2070	0.621014085
870	0.537739437	2100	0.621307042
900	0.543457746	2130	0.621525352
930	0.548797183	2160	0.621757746
960	0.553888732	2190	0.621928169
990	0.558605634	2220	0.622129577
1020	0.563040845	2250	0.622266197
1050	0.567266197	2280	0.622370423
1080	0.571185915	2310	0.622485915
1110	0.574901408	2340	0.622590141
1140	0.578346479	2370	0.622685915
1170	0.581639437	2400	0.622725352
1200	0.665355509	2430	0.62275493

the maximum ethanol uptake recorded is 48 mg. The mass uncertainty computed is 0.00938 %, and the experimental error bars would not be visible in Figure 4.

Results and Discussion

Figure 3 shows the adsorption isotherms of the ACF (A-20)/ethanol pair for temperatures ranging from 20 to 80 °C and pressures from 0 to 15 kPa, which could be needed for designing an adsorption chiller. These data are fitted with the Dubinin−Radushkevich (D−R) equation, as shown in eq 1 below

$$W = W_o \exp\left\{-D\left[T \ln\left(\frac{P_s}{P}\right)\right]^2\right\} \quad (1)$$

where W is the equilibrium uptake [kg of ethanol/kg of ACF (A-20)], P_s denotes the saturation pressure corresponding to the adsorbent temperature, P indicates the system pressure, and T stands for adsorbent temperature in Kelvin. The constants for the D−R equation have been determined experimentally in previous experiments by the same authors.[26] The values of W_o and D are 0.797 kg/kg and 1.716×10^{-6} K^{-2}, respectively.[26] As shown by the broken lines in Figure 3, the analysis of adsorption kinetics has been made for an adsorption load ranging from 0.1 to 0.5 kg of ethanol/kg of ACF and is almost a linear range.

Figure 4 shows the kinetic uptake of ethanol on the ACF (A-20) for seven assorted adsorption temperatures, namely, 27 °C, 28 °C, 31.5 °C, 35 °C, 40 °C, 50 °C, and 60 °C. These uptake data are also furnished in Tables 2 to 6. Each kinetic curve is recorded at 0.5 s intervals using the Cahn 2121 TGA apparatus (±0.1 μg) with an initial dry adsorbent mass of 71 mg, and the experiments span from 800 s for the relatively high temperatures to 2800 s for the lower temperature isotherms. Adsorption measurements are continued until they reach the equilibrium condition.

The linear driving force (LDF) equation has been widely accepted for adsorbate uptake under a constant adsorption temperature. A well-known LDF is that of Glueckauf and Coates[27] which is given by

$$\frac{\partial w}{\partial t} = k_s a_v (W - w) \quad (2)$$

where $k_s a_v$ is the overall mass transfer coefficient. The availability of measured kinetic curves, as shown in Figure 4, provides a direct method for evaluating the overall mass transfer coefficient for each isotherm. The experimental adsorption rate is measured with a time interval of 0.5 s and the instantaneous mass transfer coefficient, $(k_s a_v)_i$, can be calculated directly. The average value of the overall mass transfer coefficient ($k_s a_v$) can be estimated using the following relation

$$k_s a_v = \frac{\sum_{i=1}^{n} (k_s a_v)_i}{n} \quad (3)$$

Table 4. Experimental Uptake at 40 °C

time/s	w/kg·kg^{-1}	time/s	w/kg·kg^{-1}	time/s	w/kg·kg^{-1}	time/s	w/kg·kg^{-1}
0	0	330	0.295283099	660	0.404225352	990	0.455750704
30	0.090038028	360	0.308307042	690	0.410432394	1020	0.458192958
60	0.123819718	390	0.32055493	720	0.416504225	1050	0.460314085
90	0.151138028	420	0.332060563	750	0.422357746	1080	0.461956338
120	0.174867606	450	0.34293662	780	0.427673239	1110	0.463104225
150	0.196301408	480	0.353335211	810	0.432759155	1140	0.463783099
180	0.216011268	510	0.363008451	840	0.437543662	1170	0.464071831
210	0.234156338	540	0.372176056	870	0.441921127		
240	0.251030986	570	0.380829577	900	0.445966197		
270	0.26673662	600	0.389022535	930	0.449612676		
300	0.281460563	630	0.396807042	960	0.452870423		

Table 5. Experimental Uptake at 50 °C

time/s	w/kg·kg^{-1}	time/s	w/kg·kg^{-1}	time/s	w/kg·kg^{-1}	time/s	w/kg·kg^{-1}
0	0	270	0.221011268	540	0.305960563	810	0.359236620
30	0.076602817	300	0.232866197	570	0.313140845	840	0.363145070
60	0.105298592	330	0.243963380	600	0.319940845	870	0.366474648
90	0.127757746	360	0.254392958	630	0.326464789	900	0.369126761
120	0.147028169	390	0.264236620	660	0.332692958	930	0.371114085
150	0.164429577	420	0.273476056	690	0.338801408	960	0.372239437
180	0.180292958	450	0.282240845	720	0.344847887	990	0.372433803
210	0.194909859	480	0.290601408	750	0.349946479		
240	0.208438028	510	0.298418310	780	0.354823944		

Table 6. Experimental Uptake at 60 °C

time/s	w/kg·kg^{-1}	time/s	w/kg·kg^{-1}	time/s	w/kg·kg^{-1}	time/s	w/kg·kg^{-1}
0	0	210	0.164907042	420	0.228459155	630	0.271811268
30	0.065422535	240	0.175828169	450	0.235874648	660	0.275756338
60	0.090946479	270	0.185909859	480	0.242914085	690	0.27885493
90	0.110085915	300	0.195333803	510	0.249494366	720	0.280883099
120	0.126209859	330	0.204578873	540	0.255809859	750	0.281740845
150	0.140408451	360	0.212928169	570	0.261752113		
180	0.153125352	390	0.220891549	600	0.267094366		

where n is the number of time intervals and can be calculated by the following relation

$$n = \frac{t - t_{in}}{\Delta t} \tag{4}$$

where t denotes time, t_{in} is the initial time, and Δt is the time interval which is equal to 0.5 s. The instantaneous uptake can be derived by integrating eq 2 as shown below

$$\int \frac{\partial w}{(W - w)} = \int k_s a_v \, \partial t \tag{5}$$

$$\ln(W - w) = -k_s a_v t + C \tag{6}$$

The integration constant C is evaluated by using the initial condi tion (at $t = t_{in}$, $w = w_{in}$), where t_{in} is the required time to stabilize the system pressure and w_{in} is the uptake at time t_{in}. Substituting the value of the constant C, eq 6 can be rewritten as

$$\frac{W - w}{W - w_{in}} = \exp[-k_s a_v (t - t_{in})] \tag{7}$$

A simple mathematical rearrangement gives

$$\frac{w - w_{in}}{W - w_{in}} = 1 - \exp[-k_s a_v (t - t_{in})] \tag{8}$$

$$w = w_{in} + (W - w_{in})\{1 - \exp[-k_s a_v (t - t_{in})]\} \tag{9}$$

In eqs 2 to 9, the overall mass transfer coefficient is considered as a constant within the selected ranges of time and temperatures. The validity of this assumption is shown in Figure 5, where $w - w_{in}$ is plotted against $(W - w_{in})\{1 - \exp[-k_s a_v (t - t_{in})]\}$ for all seven assorted isotherms presented herein. It can be noticed that there is a good agreement between both of the plotted terms and hence the assumption of $K_s a_v$ as a constant value for each of the isotherms is justified.

The relationship between the overall mass transfer coefficient ($k_s a_v$) and the diffusion time constant (D_s/R_p^2) is given by the LDF equation via the constant F_o, that is

$$K_s a_v = \frac{F_o D_s}{R_p^{\,2}} \tag{10}$$

where D_s is the intraparticle surface diffusion. Employing the cylindrical model for ACF, the numerical value of F_o is estimated to be 11 for the ACF (A-20)/ethanol pair within the selected operating temperature and time ranges.[28] As the overall mass transfer coefficient depends on the surface diffusion, the classical Arrhenius equation is sufficient to describe its sensitivity to the activation energy, adsorbent radius, and temperature,[29] that is

$$D_s = D_{so} \exp\left(\frac{-E_a}{RT}\right) \tag{11}$$

where the right-hand side terms can be rearranged as

$$\ln(D_s) - \ln(D_{so}) = \left(\frac{-E_a}{RT}\right) \tag{12}$$

By plotting $\ln(D_s)$ with respect to $1/T$, known as the Arrhenius plot, one can get the numerical values of the activation energy E_a and the preexponential constant D_{so}, which are shown in Figure 6. As can be noticed from Figure 6, the Arrhenius plot has a good linear relationship. The intercept provides the value

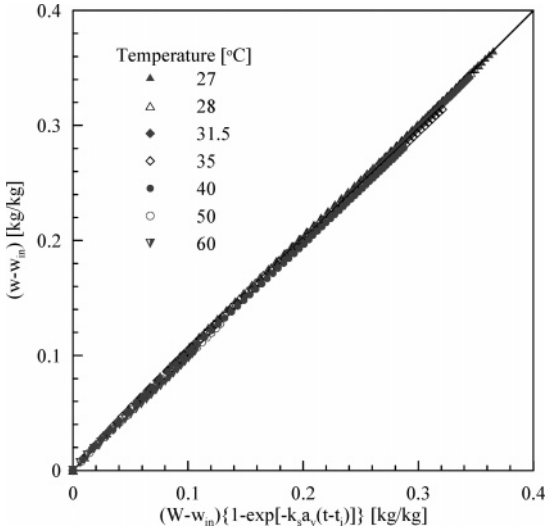

Figure 5. Plot of $(w - w_{in})$ vs $(W - w_{in})\{1 - \exp[-k_s a_v(t - t_{in})]\}$ for all seven isotherms.

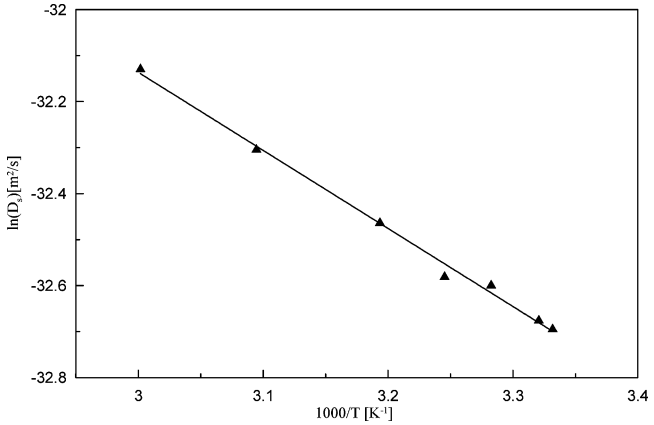

Figure 6. Arrhenius plot of the ACF(A-20)/ethanol pair.

of the preexponential constant D_{so} of eq 11 and the slope gives the activation energy, E_a. For the ACF (A-20), the numerical values of D_{so} and E_a are 1.8×10^{-12} and 306.7 kJ·kg^{-1}, respectively. This activation energy, E_a, has been found experimentally to fall in the range of the relation defined by Carman,[30] which is shown in eq 13, below.

$$0.3 \times Q_{st} < E_a < 1.0 \times Q_{st} \qquad (13)$$

Here, Q_{st} is the heat of adsorption which is experimentally found to be 1006 kJ·kg^{-1}.[31] This implies that the activation energy is about 30 % of the heat of adsorption. The activation energy falls in the lower region of the relation defined by Carman[30] as ethanol is a volatile substance. Similar low activation energy that is almost about 30 % of the adsorption heat for O_2 adsorption on the $K_2SO_4-Ag/\alpha\text{-}Al_2O_3$ catalyst has also been reported by Ayame et al.[32] It can also be noted that, when the adsorption rate is controlled by an intraparticle diffusion mechanism, the activation energy is very low and hence the adsorption process is controlled by intraparticle diffusion which is a physical step in the adsorption process.[33]

A comparison between experimentally measured and predicted adsorption rates are shown in Figure 7, where the measured adsorption rates are determined by applying a finite difference scheme on the TGA data while the predictions are obtained by back substitutions of eqs 11, 10, and 9 into eq 2. A good agreement for the adsorption rates is observed, and the

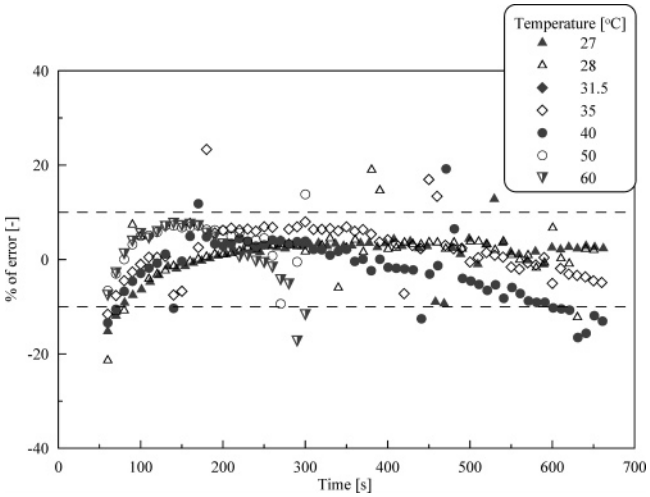

Figure 7. Comparison between experimental and predicted adsorption rates.

maximum percentage error for the bulk data (from seven isotherms) is found to be within ±10 %.

Conclusions

The mass uptake of ethanol on ACF (A-20) has been studied under a controlled pressure and temperature environment using a thermogravimetric analyzer. It has been observed that the kinetic curves have rapid adsorption rates at the early stage of transients. With the same measured kinetics, the overall mass transfer coefficients have been computed with respect to time and the instantaneous uptake of ethanol. From the LDF model, the log−linear plot of surface diffusion vs the reciprocal of temperature gives the classical Arrhenius model where the analysis of the intercept and gradient yield the respective values of activation energy (E_a) and the preexponential constant (D_{so}). The experimental data and predicted results show satisfactory agreement.

From the present study, the ACF (A-20)/ethanol pair is deemed suitable for adsorption chiller design and a large refrigeration capacity can be expected from the adsorption cycle.

Literature Cited

(1) Zhu, W.; Gora, L.; van den Berg, A. W. C.; Kapteijn, F.; Jansen, J. C.; Moulijn, J. A. Water vapour separation from permanent gases by a zeolite-4A membrane. *J. Membr. Sci.* **2005**, *253* (1−2), 57−66.

(2) Xu, X.; Yang, W.; Liu, J.; Lin, L. Synthesis of NaA zeolite membrane by microwave heating. *Sep. Purif. Technol.* **2001**, *25* (1−3), 241−249.

(3) Aoki, K.; Kusakabe, K.; Morooka, S. Separation of gases with an A-type zeolite membrane. *Ind. Eng. Chem. Res.* **2000**, *39*, 2245−2251.

(4) Hagiwara, K.; Yonedu, S.; Saito, K.; Shiraishi, T.; Sugo, T.; Tojyo, T.;Katayama, E. High-performance purification of gelsolin from plasma using anion-exchange porous hollow-fiber membrane. *J. Chromatogr., B: Biomed. Sci. Appl.* **2005**, *821* (2), 153−158.

(5) Huo, J.; Liu, H.; Qu, J.; Wang, Z.; Ge, J.; Liu, H. Preparation and characteristic of triolein-embedded composite sorbents for water purification. *Sep. Purif. Technol.* **2005**, *44* (1), 37−43.

(6) Hidayat, C.; Takagi, M.; Yoshida, T. Expanded bed adsorption for purification of alcohol dehydrogenase using a dye-iminodiacetic acid matrix. *J. Biosci. Bioeng.* **2004**, *97* (4), 284−287.

(7) Hildbrand, C.; Dind, P.; Pons, M.; Buchter, F. A new solar powered adsorption refrigerator with high performance. *Sol. Energy* **2004**, *77* (3), 311−318.

(8) Sakoda, A.; Suzuki, M. Fundamental study on solar powered adsorption cooling system. *J. Chem. Eng. Jpn.* **1984**, *17* (1), 52−57.

(9) Saha, B. B.; Koyama, S.; Kashiwagi, T.; Akisawa, A.; Ng, K. C.; Chua, H. T. Waste heat driven dual-mode, multi-stage, multi-bed regenerative adsorption system. *Int. J. Refrig.* **2003**, *26* (7), 749−757.

(10) Saha, B. B.; Koyama, S.; Lee, J. B.; Kuwahara, K.; Alam, K. C. A.; Hamamoto, Y.; Akisawa, A.; Kashiwagi, T. Performance evaluation

of a low-temperature waste heat driven multi-bed adsorption chiller. *Int. J. Multiphase Flow* **2003**, *29* (8), 1249−1263.
(11) Prakash, M. J.; Prasad, M.; Rastogi, S. C.; Akkimaradi, B. S.; Gupta, P. P.; Narayanamurty, H.; Srinivasan, K. Development of a laboratory model of activated charcoal-nitrogen adsorption cryocooler. *Cryogenics* **2000**, *40* (7), 481−488.
(12) Duband, L.; Collaudin, B. Sorption coolers development at CEA-SBT. *Cryogenics* **1999**, *39* (8), 659−663.
(13) Li, S.; Pan, W.; Mao, Z. A comparative study of the electrochemical hydrogen storage properties of activated carbon and well-aligned carbon nanotubes mixed with copper. *Int. J. Hydrogen Energy* **2005**, *30* (6), 643−648.
(14) Liu, C.; Yang, Q. H.; Tong, Y.; Cong, H. T.; Cheng, H. M. Volumetric hydrogen storage in single-walled carbon nanotubes. *Appl. Phys. Lett.* **2002**, *80* (13), 2389−2391.
(15) Yang, R. T. Hydrogen storage by alkali-doped carbon nanotubes-revisited. *Carbon* **2000**, *38* (4), 623−626.
(16) Kowalczyk P.; Gunko, V. M.; Terzyk, A. P.; Gauden, P. A.; Rong, H.; Ryu, Z. The comparative characterization of structural heterogeneity of mesoporous activated carbon fibers (ACFs). *Appl. Surf. Sci.* **2003**, *206* (1−4), 67−77.
(17) Park, S. J.; Jang, Y. S.; Shim, J. W.; Ryu, S. K. Studies on pore structures and surface functional groups of pitch-based activated carbon fibers. *J. Colloid Interface Sci.* **2003**, *260* (2), 259−64.
(18) Lee, Y. S.; Basova, Y. V.; Edie, D. D.; Reid, L. K.; Newcombe, S. R.; Ryu, S. K. Preparation and characterization of trilobal activated carbon fibers. *Carbon* **2003**, *41* (13), 2573−84.
(19) Ryu, S. K.; Jin, H.; Gondy, D.; Pusset, N.; Ehrburger, P. Activation of carbon fibers by steam and carbon dioxide. *Carbon* **1993**, *31* (5), 841−842.
(20) Suzuki, M. Activated carbon fiber: fundamentals and applications. *Carbon* **1994**, *32* (4), 577−586.
(21) Saha, B. B.; Koyama, S.; Alam, K. C. A.; Hamamoto, Y.; Akisawa, A.; Kashiwagi, T.; Ng, K. C.; Chua, H. T. Isothermal adsorption measurement for the development of high performance solid sorption cooling system. *Trans. JSRAE* **2003**, *20* (3), 421−427.
(22) Takeuchi, Y.; Shigeta, A.; Iwamoto, H. Adsorption of solvent vapor mixture in air by activated carbon fiber bed. *Sep. Technol.* **1993**, *3* (1), 46−52
(23) Wang, R. Z.; Jia, J. P.; Zhu, Y. H.; Teng, Y.; Cheng, J.; Wang, Q. B. Study on a new solid adsorption refrigeration pair: activated carbon fiber − methanol. *J. Sol. Energy Eng.* **1997**, *119*, 214−218.
(24) Cui, Q.; Tao, G.; Chen, H.; Guo, X.; Yao, H. Environmentally benign pairs for adsorption refrigeration. *Energy* **2005**, *30* (2−4), 261−271.
(25) Kanamori, M.; Hiramatsu, M.; Katsurayama, K.; Watanabe, F.; Matsuda, H.; Hasatani, M. Production of cold heat energy by alcohol/activated carbon adsorption heat pump with a disk-module-type adsorber. *J. Chem. Eng. Jpn.* **1997**, *30* (3), 434−439.
(26) El-Sharkawy, I. I.; Kuwahara, K.; Saha, B. B.; Koyama, S.; Ng, K. C. Experimental investigation of activated carbon fibers/ethanol pairs for adsorption cooling system application. *Appl. Therm. Eng.* **2006**, *26* (8−9), 859−865.
(27) Glueckauf, E.; Coates, J. E. Theory of chromatography IV. *J. Chem. Soc.* **1947**, 1315−1321.
(28) El-Sharkawy, I. I.; Saha, B. B.; Koyama, S.; Ng, K. C. A study on the kinetics of ethanol-activated carbon fiber: theory and experiments, *Int. J. Heat Mass Transfer* **2006**, *49* (17−18), 3104−3110.
(29) Glueckauf, E. Formula for diffusion into sphere and their application to chromatography. *Trans. Faraday Soc.* **1955**, *51*, 1540−1551.
(30) Carman, P. C. In *Flow of Gases Through Porous Media*; Academic Press: New York, 1956.
(31) El-Sharkawy, I. I.; Saha, B. B.; Kuwahara, K.; Koyama, S.; Ng, K. C. Fundamental characteristics of adsorption cooling cycle using activated carbon fiber/ethanol pair. *4th International Conference on Heat Transfer, Fluid Mechanics and Thermodynamics*, Paper No. EI1, Cairo, Egypt, 2005.
(32) Ayame, A.; Eimaeda, S.; Feng, L.; Hayasaka, H. Oxygen adsorption on silver catalysts during the course of partial oxidation of ethylene. *Appl. Catal., A* **2006**, *304*, 93−108.
(33) Sismanoglu, T.; Pura, S. Adsorption of aqueous nitrophenols on clinoptilolite. *Colloids Surf., A* **2001**, *180*, 1−6.

Received for review February 20, 2006. Accepted July 4, 2006. The authors acknowledge the financial support under the ASTAR/SERC grant of Singapore (Project No. 0221010035).

JE060071Z